Acta Biochim Biophys Sin 2025, 57(6): 995–1005
https://cstr.cn/32197.14.abbs.2024210
https://doi.org/10.3724/abbs.2024210
Original Article

Original Article

Ivermectin inhibits the growth of ESCC by activating the ATF4-mediated endoplasmic reticulum stress-autophagy pathway

Huiyang Liu[1], Zhirong Chai[1], Ya Gao[1], Yanming Wang[2,*], and Mengmeng Lu[1,3,*]

[1]Epigenetics & Translational Medicine Laboratory, School of Life Sciences, Henan University, Kaifeng 475004, China, [2]The First Affiliated Hospital of Henan University, Henan University, Kaifeng 475004, China, and [3]State Key Laboratory of Antiviral Drugs, School of Pharmacy, Henan University, Kaifeng 475004, China

*Correspondence address. Tel: +86-13137587721; E-mail: mengmenglu@vip.henu.edu.cn (M.L.) / Tel: +86-15684536727; E-mail: yanmingwang@henu.edu.cn (Y.W.)

Received 10 August 2024 Accepted 17 October 2024 Published 22 November 2024

Abstract

Esophageal squamous cell carcinoma (ESCC) is one of the most common forms of malignancy worldwide. However, there is currently a lack of effective chemotherapeutic drugs for ESCC. Ivermectin is a broad-spectrum antiparasitic drug with notable antitumor activity. However, the cellular and molecular mechanisms by which ivermectin inhibits cancer growth remain unclear. In this study, we elucidate the role of ivermectin in ESCC suppression by activating the endoplasmic reticulum (ER) stress and autophagy pathways. In transcriptome analyses, we find that activating transcription factor 4 (ATF4) and DNA damage inducible transcript 3 (DDIT3) are involved in the activation of ER stress by ivermectin. Moreover, ivermectin treatment suppresses the growth of ESCC xenograft tumors in nude mice. Taken together, our results establish the antitumor molecular role of ivermectin in targeting the ER stress-autophagy pathway and suggest that ivermectin is a potential drug candidate for the treatment of ESCC.

Key words ivermectin, ESCC, ER stress, ATF4, autophagy

Introduction

Esophageal cancer is a serious malignant gastrointestinal disease [1], with a global incidence of approximately 500,000 new cases per year, and more than half of these cases occur in China [2]. Esophageal squamous cell carcinoma (ESCC) is the main pathological type and accounts for approximately 90% of all esophageal cancer cases in China [3]. The primary treatment for esophageal cancer is surgery. However, due to a lack of early diagnosis, chemotherapy is an important option for the treatment of many inoperable patients [4]. Chemotherapy is associated with many side effects because of the side effects of the many currently used drugs, highlighting the need for new therapeutic agents.

Ivermectin is a safe and efficacious drug approved by the Food and Drug Administration (FDA) for clinical application. Ivermectin has the highest antiparasitic activity, is safe among avermectins, and has been studied as an antiviral or antineoplastic alternative [5,6]. As an antiparasitic drug, ivermectin primarily antagonizes the closure of glutamate-gated chloride channels, causing hyperpolarization of nerve and muscle cells in invertebrates, which in turn paralyzes the pharynx and leads to death [7]. As an alternative antiviral agent, ivermectin inhibits the importin α/β1-mediated nuclear import of viral proteins [8,9]. Many studies have shown that ivermectin exerts antitumor effects on cancers [10,11]. However, the antitumor molecular mechanisms of ivermectin are complex and poorly understood. In addition, studies on the mechanism of action of ivermectin in ESCC are scarce, and the potential benefits of ivermectin in ESCC therapy are underexplored.

Autophagy is a fundamental cell biology pathway that is involved in many pathological and physiological processes [12], which can be increased in response to cellular stresses, such as elevated ER stress, to maintain cellular homeostasis [13]. Moreover, the ER-stress leads to the release of Ca^{2+} from the ER into the cytosol, leading to the activation of the CaMKK-b, AMPK, and mTOR pathways, which in turn activate autophagy [14]. LC3 and p62

(sequestosome 1, SQSTM1) serve as markers of autophagy. The generation of phagophores and autophagosomes is linked to the lipidation of LC3 I with phosphatidylethanolamine, resulting in the formation of the membrane-bound LC3 II protein [12]. The cellular level of p62 is inversely correlated with the rate of autophagic vesicle degradation because of its selective degradation during autophagy [12]. ER stress induces autophagy flux in tumor cells [15].

ER stress is one of the conditions that may induce autophagy. When many unfolded proteins accumulate, cells initiate autophagy, leading to the degradation of the unfolded proteins [16]. Since ER stress plays an important role in cancer biology, understanding the mechanism of ER stress-mediated autophagy pathways is pivotal [17]. In addition, ER stress is closely linked to the sensitivity of ESCC to chemotherapeutic agents [17]. Activating transcription factor 4 (ATF4) promotes the transcription of many stress-activated genes and is considered a master stress response regulator [18]. ATF4 increases the transcription of DNA damage inducible transcript 3 (DDIT3) / C/EBP homologous protein (CHOP), which is an important partner of ATF4 that induces apoptosis [18]. In response to ER stress, protein kinase R (PKR)-like endoplasmic reticulum kinase (PERK) phosphorylates eIF2α, leading to a selective increase in the translation of ATF4 [19]. In addition, a cohort of downstream target genes involved in cell survival, reactive oxygen species (ROS), energy homeostasis, autophagy, apoptosis and aging are upregulated by ATF4 [20–22]. It is therefore pivotal to understand the molecular mechanisms underlying the regulation of ER stress, autophagy, and apoptosis to design better strategies for cancer treatment.

Here, we show that ivermectin activates the expression of ATF4, a regulator of the ER stress pathway. Furthermore, early treatment with ivermectin promotes autophagy, whereas prolonged treatment leads to the death of ESCC cells. As such, our results establish a novel link between the ER stress-autophagy pathway and cell death.

Materials and Methods

Cell culture

Human esophageal squamous carcinoma cell lines (KYSE30, KYSE70) and human normal esophageal cells (Het-1A) were obtained from Cobioer Co. Ltd (Nanjing, China). The cells were cultured at 37°C in RPMI (01-100-1A; Biological Industries, Beit Haemek, Israel) supplemented with 10% fetal bovine serum (04-001-1A; Biological Industries), 100 U/mL penicillin and 100 μg/mL streptomycin (P1400; Solarbio Science & Technology Co. Ltd., Beijing, China).

Chemicals and antibodies

Ivermectin (HY-15310) and chloroquine (HY-17589A) were obtained from MedChemExpress (New Jersey, USA). Hydroxypropyl-beta-cyclodextrin (MB1904) was obtained from Dalian Meilun Biological Technology Co. Ltd. (Dalian, China). Antibodies against ATF4 (#11815S), LC3B (#83506S), PERK (#3192S), elF2α (#5324T), and phospho-eIF2α (Ser51) (#3398T) were purchased from Cell Signaling Technology, Inc. (CST; Boston, USA). The antibody against CHOP (15204-1-AP) was purchased from proteintech (Rosemont, USA). Anti-phospho-PERK (Thr980) (bs-3330R) was obtained from Beijing Bioss Antibodies Biological Technology Co. Ltd. (Beijing, China). Anti-Cyclin D1 (#ab16663) and anti-Cyclin E1 (#ab33911) antibodies were obtained from Abcam (Cambridge, USA). Anti-Ki67 (#CY5542) and anti-β-actin (#AB0035) antibodies were purchased from Abways (Shanghai, China). The antibody against GRP78 (#AF0171) was obtained from Beyotime (Shanghai, China). The antibody against GAPDH (#YM3029) was obtained from ImmunoWay (Plano, USA). Secondary antibodies used in western blot were HRP-conjugated anti-rabbit (111-035-003; Jackson ImmunoResearch, Langcaster, USA) and HRP-conjugated anti-mouse (115-035-003; Jackson ImmunoResearch). Secondary antibodies used in immunofluorescence was goat anti-mouse IgG H&L (Alexa Fluor® 647) (ab150115; Abcam).

Measurement of cell viability, colony formation, and EdU incorporation

The effects of ivermectin on tumor cell growth were assessed via the 3-(4,5-dimethylthiazol-2-yl)-2,5-diphenyl tetrazolium bromide (MTT) assay as described previously [23]. In detail, ESCC cells were cultured in 96-well culture plates at a density of 6×10^3 cells per well with 90 μL of RPMI supplemented with 10% FBS with antibiotics and cultured in a 37°C incubator supplemented with 5% CO_2 for 24 h. Then, 10 μL of RPMI containing the indicated concentration of ivermectin (0, 5, 10, or 15 μM) was added. At 48 h after ivermectin treatment, 10 μL of MTT reagent (M8180; Solarbio Science & Technology Co. Ltd, Beijing, China.) was added to each well and incubated for 4 h. Subsequently, the liquid supernatant was removed and replaced by 100 μL of DMSO to dissolve the formazan crystals. The OD values were measured at 570 nm via a multifunctional microplate reader (SynergyNeo2; BioTek Instruments Inc., Winooski, USA). The cell viabilities are presented as percentages of the control cells. The experiments were performed in triplicate.

The long-term effects of ivermectin on tumor cell proliferation were analyzed via colony formation assay. ESCC cells were seeded at a density of 600 cells/well in 6-well plates and cultured for 3 days before starting treatment with ivermectin (0, 5, 10, or 15 μM). The medium was changed every 72 h. After 7 days of treatment, the colonies were fixed with formaldehyde, stained with crystal violet for 15 min and washed three times. The visible colonies were photographed with an Amersham imager 680 (GE, Healthcare Bio-Sciences AB, Uppsala, Sweden).

DNA replication was measured via a Cell Proliferation EdU Kit (KTA2030; Abbkine Inc., Wuhan, China). ESCC cells were seeded into a 96-well plate at a final volume of 100 μL/well. The cells were treated with various concentrations of ivermectin in a 37°C incubator supplemented with 5% CO_2. After 24 h, 10 μM EdU in serum-free medium was added to the treated cells, followed by incubation for 4 h. The EdU-labeled cells were fixed and then incubated with Click-iT reaction mixture for 30 min at room temperature in the dark. The cells were washed and stained with Hoechst 33342 (C0030; Solarbio Science & Technology Co. Ltd.). The samples were analyzed for green fluorescence for EdU labeling and blue fluorescence for DNA labeling with a fluorescence microscope (Axio observer; Carl Zeiss, Oberkochen, Germany).

RNA-Seq library preparation and gene expression quantification

Total RNA samples were extracted using the TRIzol reagent (Invitrogen, Carlsbad, USA). The RNA concentrations were quantified with an Agilent 2100 instrument (Agilent Technologies, Palo Alto, USA). RNA-Seq libraries were constructed via the TruSeq

Stranded mRNA Library Prep Kit (Illumina, San Diego, USA). Sequencing was performed on an Illumina HiSeq platform with a 2×150 bp paired-end (PE) configuration. The sequences were processed and analyzed by GENEWIZ. After sequencing, the raw sequencing reads were processed via Cutadapt (V1.9.1) to obtain high-quality clean data. The reference genome sequence for *Homo sapiens* (hg19) was downloaded from the UCSC website (https://hgdownload.soe.ucsc.edu/goldenPath/hg19/bigZips/?C=N;O=D). The clean data were aligned to the reference genome via HISAT2 software (v2.0.1). The DESeq2 package was used for differential expression analysis, and the adjusted *P* value of genes was set at <0.05 to detect differentially expressed genes. Source codes for DESeq2 and volcano images are available on GitHub (https://github.com/mengmenglu721/ivermectin.git).

GO, KEGG and GSEA enrichment analysis

GOSeq (v1.34.1) was used to identify Gene Ontology (GO) terms that annotate a list of enriched genes (adjusted *P*-value <0.05). Kyoto Encyclopedia of Genes and Genomes (KEGG) analysis was used to analyze the enriched pathways of the candidate genes (http://en.wikipedia.org/wiki/KEGG) (Qvalue <0.05). Further gene set enrichment analysis was performed using Gene Set Enrichment Analysis (https://www.gsea-msigdb.org/gsea/index.jsp).

Flow cytometry analysis

Apoptosis was detected via an Annexin V-FITC/PI Apoptosis Detection Kit (P-CA-201; Procell Life Science & Technology Co. Ltd., Wuhan, China). Briefly, ESCC cells were incubated with ivermectin (0, 5, 10, or 15 μM) for 24 h or 48 h. ESCC cells (5×10^6) were harvested after centrifugation (129 g, 5 min) and washed 3 times. In accordance with the instructions of the kit, the cells were resuspended in 500 μL of binding buffer containing 5 μL of annexin V-FITC and 5 μL of PI for 15 min in the dark. The cells were subsequently analyzed with a Cytoflex flow cytometer (Beckman Coulter Inc., Pasadena, USA).

Determination of the intracellular ROS concentration

The intracellular ROS levels were examined via a DCFH-DA kit (CA1410; Solarbio Science & Technology Co. Ltd.). ESCC cells were cultured with ivermectin (0, 5, 10, or 15 μM) in 6-well plates at a density of 1.5×10^5 cells per well for 6 h. The cells were washed with PBS and incubated with DCFH-DA in serum-free medium at 37°C for 10 min. After incubation, the cells were washed 3 times with PBS and analyzed with a Cytoflex flow cytometer (Beckman Coulter Inc.).

Determination of intracellular Ca^{2+} concentrations

The intracellular free Ca^{2+} concentration was measured with Fluo-4 AM (S1060; Beyotime) according to the manufacturer's instructions. In detail, the cells were treated with different doses of ivermectin for 24 h at 37°C under 5% CO_2. Before the cells were incubated with Fluo-4 AM (final concentration of 1 μM), they were washed three times with HBSS (H1025; Solarbio Science & Technology Co. Ltd.). After incubation for 30 min in PBS at 37°C, the intensity of the fluorescence was obtained via a flow cytometer by measuring the emission at 488 nm.

Cell cycle analysis

A cell cycle analysis kit (C6031; Yuheng Biotechnology Co. Ltd., Suzhou, China) was used to analyze the ivermectin-treated ESCC cells. The cells were seeded in 6-well plates and then treated with 0, 5, 10, or 15 μM ivermectin for 24 h in a 37°C incubator supplemented with 5% CO_2. The cells were collected and fixed in 70% ethanol at 4°C overnight after being washed with PBS. The cells were resuspended in binding buffer with RNase A and stained with PI for 20 min in the dark. The fluorescent signal was analyzed with a Cytoflex flow cytometer (Beckman Coulter Inc.).

Western blot analysis

Proteins were extracted from whole cells with RIPA lysis buffer (PC101; Epizyme Biotech, Shanghai, China) supplemented with a protease inhibitor cocktail (M5293; AbMole BioScience, Houston, USA), after which the protein concentration was determined with a BCA kit (CW0014; CWBIO Corporation, Beijing, China). The sample was then separated by 10% or 12.5% SDS-PAGE and subsequently electro-transferred to a PVDF membrane (Millipore, Bedford, USA). The membrane was blocked for half an hour with 5% nonfat milk. After blocking, the membrane was incubated with primary antibodies at 4°C overnight, followed by incubation with appropriate secondary antibodies, and then signals were detected with an Amersham imager 680 (GE) using enhanced chemiluminescence (ECL) reagent (SQ201; Epizyme Biotech, Shanghai, China).

RT-PCR analysis

RNA was extracted via a Gene JET RNA purification kit (K0731; Thermo Fisher Scientific Inc., Waltham, USA). Reverse transcription was performed via an RT first-strand cDNA synthesis kit (G3330; Servicebio Technology Co. Ltd., Wuhan, China). PCR was performed with 2× SYBR green (G3321; Servicebio Technology Co. Ltd.) in an Applied Biosystems Quantstudio 5 (Thermo Fisher Scientific Inc.). The primers used are listed in Supplementary Table S1. Gene expression levels were normalized to the expression of *β-actin*.

Live-cell imaging of mCherry-GFP-LC3 and GFP-LC3

KYSE30 cells were cultured in glass-bottom dishes. The cells were transfected with the GFP-LC3 or mCherry-GFP-LC3 reporter plasmid. The transfection was performed via the INVI DNA/RNA Transfection Reagent (IV1216150; Invigentech, Irvine, USA) in serum-free medium. The cells were cultured for 8 h after transfection before the addition of ivermectin to complete culture medium. After incubation with ivermectin for 24 h, the nuclei were stained with Hoechst 33342. Live-cell images were captured via a Nikon Til 2 confocal laser scanning microscope (Nikon, Tokyo, Japan).

Transmission electron microscopy (TEM)

After ivermectin treatment as indicated, the ESCC cells were fixed in electron microscope fixative (G1102; Servicebio Technology Co. Ltd.). A Leica UC7 microtome (Leica, Heidelberg, Germany) was used to prepare ultrathin sections after dehydration. TEM imaging was performed with an HT7800 transmission electron microscope (Hitachi Ltd., Tokyo, Japan).

Knockout of *ATF4* with CRISPR-Cas9 ($ATF4^{-/-}$) and forced expression of ATF4

A CRISPR knockout method against *ATF4* was used. The gRNAs were designed on the website (https://zlab.bio/guide-design-resources; Supplementary Table S1). To overexpress ATF4, ESCC

cells were transfected with the pLenti-v3-hATF4 plasmid. 293T cells were used for virus packaging. Transfection reagent, the envelope plasmid pMD2.G, and the packaging plasmid psPAX2 was used together with the gRNA plasmid or the pLenti-v3-hATF4 plasmid. Transfection complexes were prepared in serum-free growth medium. The cells were maintained for 12 h in serum-free medium before they were returned to the growth medium. The cell supernatant was collected at 24 h and 48 h after transfection. The virus supernatants were filtered through a 0.22-μm membrane filter. The ESCC cells were transfected with the virus supernatant twice before selection with 1 μg/mL puromycin (Santa Cruz Biotechnology, Santa Cruz, USA). Selected cells of single cell colony (KYSE30 ATF4$^{-/-}$) or mixed cells (KYSE30 ATF4) (puromycin resistant) were screened for the expression of ATF4 via Sanger sequencing, qPCR and western blot analysis.

Animal models

The tumor xenografts were established in 6-week-old male BALB/c nude mice obtained from Nanjing GemPharmtech Co., Ltd. (Nanjing, China). All animal experiment procedures were approved by the Henan University Institutional Animal Care and Use Committee (Approval number: HUSOM2020-171). For the tumor growth model, 5×10^6 KYSE30 cells were resuspended in PBS and engrafted in the right oxter of nude mice. When the tumor volume reached approximately 70 mm^3, the mice were randomized into two groups and intraperitoneally injected with 10 mg/kg ivermectin ($n = 6$) or vehicle alone (10% hydroxypropyl-beta-cyclodextrin, $n = 6$). Tumor volume (volume in mm^3 = L × W^2/2) and body weight (g) were measured. To euthanize the mice, they were subjected to carbon dioxide asphyxiation. The tumor tissues were weighed and fixed in formaldehyde for subsequent analysis. We stated that the study was reported in accordance with the ARRIVE guidelines.

Immunofluorescence microscopy

Tumor tissues were put into 4% paraformaldehyde and fixed for 24 h at room temperature. The fixed tissues were dehydrated, imbedded in paraffin, and cut into sections. The sections were baked at 65°C for 2 h and soaked in xylene to remove paraffin. Next, the sections were rehydrated through a graded ethanol series. The sections were preincubated with 5% BSA for 30 min. The sections were incubated with antibodies against Ki67 (#CY5542; Abways) overnight at 4°C. The sections were incubated with Alexa Fluor 647 (ab150115; Abcam) secondary antibodies for 2 h at 37°C and adding DAPI solution (10 μg/mL) to stain for nuclei. The fluorescence images were captured using a fluorescence microscope (Axio observer; Carl Zeiss).

Statistical analysis

Data were statistically analyzed via one-way ANOVA via SPSS software (SPSS Statistics, V11.5; IBM, Armonk, USA). The images were analyzed using Image J (NIH, Bethesda, USA). The results are presented as the mean ± standard deviation (SD). $P < 0.05$ was considered statistically significant.

Results

Ivermectin suppresses the growth of ESCC *in vitro* and *in vivo*

To assess the anticancer effect of ivermectin on ESCC cells, MTT assays were conducted. Ivermectin decreased the viability of ESCC KYSE30 and KYSE70 cells in a dose-dependent manner (Figure 1A and Supplementary Figure S1A,B). A lower concentration of ivermectin (2.5–10 μM) had no cytotoxic effect in non-cancerous esophageal Het-1A cells (Supplementary Figure S1C), suggesting that ivermectin is more cytotoxic to cancer cells. A reduced clonogenic ability was observed after ivermectin treatment in KYSE30 cells (Figure 1B). Moreover, significantly lower percentages of EdU-positive cells were observed after ivermectin treatment (Figure 1C). The above results indicated that ivermectin suppressed the proliferation of ESCC cells *in vitro*.

To analyze the effects of ivermectin on the cell cycle, we performed flow cytometry analyses. After ivermectin treatment for 24 h, the percentage of KYSE30 cells in the G1 phase was increased (Figure 1D,E). Western blot analysis revealed that the levels of cyclin D1 and cyclin E1 were decreased after ivermectin treatment (Figure 1F and Supplementary Figure S2). In addition, apoptosis was induced after 48 h of ivermectin treatment (Supplementary Figure S1D). In contrast, treatment with ivermectin for 24 h had no obvious effect on the induction of KYSE30 cell apoptosis (Supplementary Figure S1E). These results suggested that ivermectin treatment blocked the transition from the G1 phase to the S phase of the cell cycle at early treatment time points, whereas longer treatment stimulated apoptosis.

To probe the effect of ivermectin on KYSE30 growth *in vivo*, we analyzed the growth of tumors in a mouse xenograft model. Compared with those in the vehicle-treated group, the tumors in the ivermectin-treated group grew at a slower rate (Figure 1G). The weights of the control tumors were greater than those of the ivermectin-treated tumors (Figure 1H,I). The body weight gain of the ivermectin treatment group exceeded that of the control group after ivermectin treatment for 20 days (Supplementary Figure S3A), whereas the spleen and liver weight-to-body weight ratios were not significantly different (Supplementary Figure S3B), suggesting that the dosage of ivermectin applied had no significant adverse effects. The xenograft tumor sections were stained for Ki67 to analyze the change in the proliferation rate of the tumor cells (Supplementary Figure S3C). Control xenograft tumors displayed stronger Ki67 staining than those in the ivermectin treatment group. Taken together, these data suggested that ivermectin inhibits tumor growth *in vivo*.

Ivermectin induces autophagy in ESCC

Next, we analyzed the cellular effects of ivermectin on ESCC cells. An increase in LC3 II after ivermectin treatment was observed in KYSE30 cells, suggesting that autophagic vesicle formation was induced after ivermectin treatment (Figure 2A). Ivermectin increased the expression of p62/SQSTM1 in a dose-dependent manner (Figure 2A,B and Supplementary Figure S4), suggesting that the p62/SQSTM1 degradation rate was lower than its rate of synthesis. Moreover, immunofluorescence staining revealed an increase in the number of LC3 puncta (Figure 2C). Using the mCherry-GFP-LC3 reporter, we detected an increase in the formation of both yellow fluorescent autophagosomes and red fluorescent autolysosomes, suggesting an increase in the autophagic flux rate in ivermectin-treated ESCC cells (Figure 2D). TEM analysis revealed significant accumulation of autophagosomes/autolysosomes in the cells after ivermectin treatment compared with the vehicle-treated cells (Figure 2E,F). Moreover, chloroquine (CQ) treatment partially restored cell growth in ivermectin-treated cells (Figure 2G), with

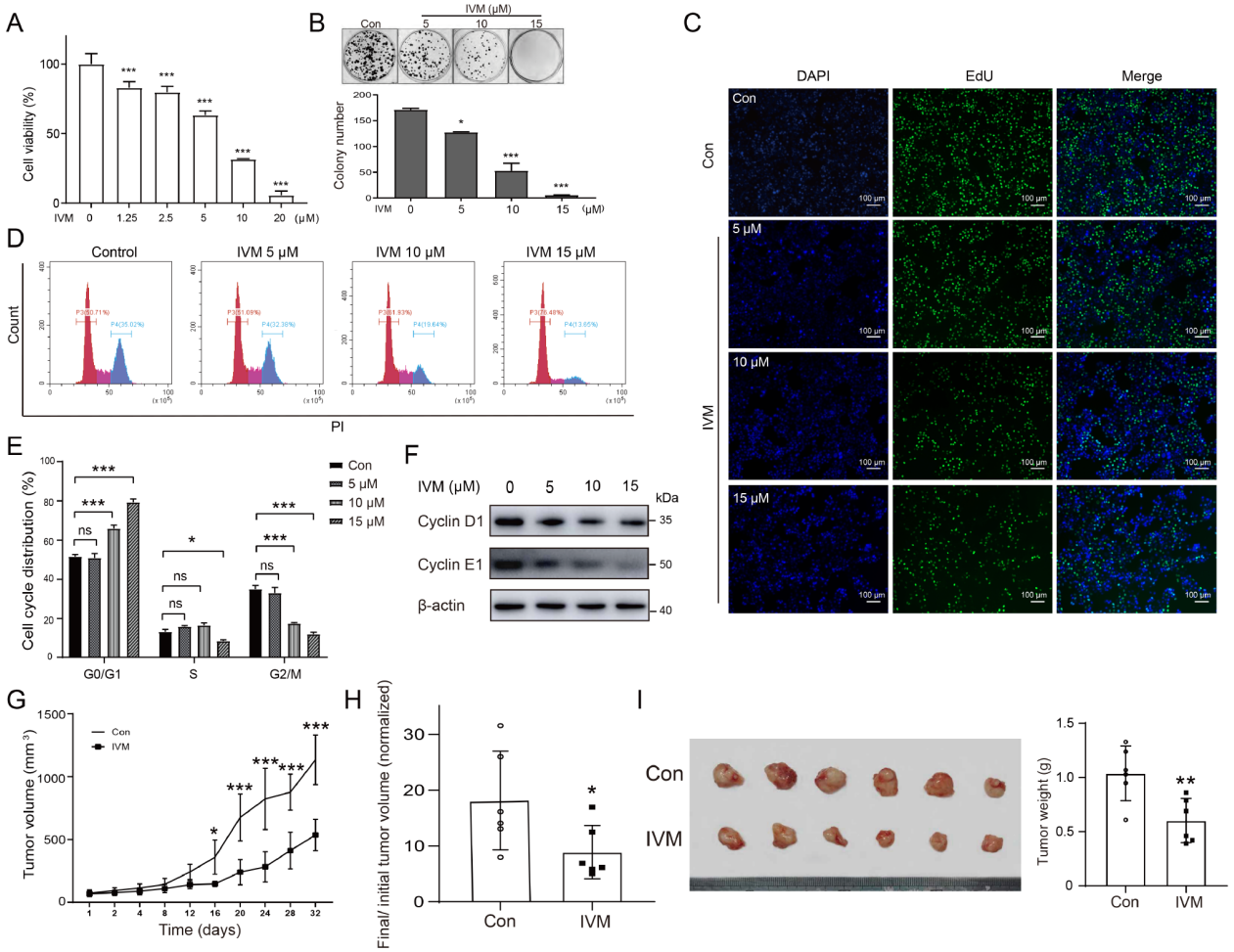

Figure 1. Ivermectin inhibits the growth of ESCC cells (A) Cell viability was measured via the MTT assay in KYSE30 cells treated with the indicated concentrations of ivermectin. ***$P < 0.001$, $n = 3$. (B) Ivermectin suppressed colony formation in KYSE30 cells. The cells were cultured with the indicated concentrations of ivermectin for 7 days. *$P < 0.05$, $n = 3$; ***$P < 0.001$, $n = 3$. (C) Inhibition of ESCC cell proliferation by ivermectin was measured via EdU labeling. Scale bar: 100 μm. (D) The cell cycle profiles of KYSE30 cells were detected by flow cytometry after incubation with ivermectin (0, 5, 10, or 15 μM). (E) Changes in KYSE30 cells during the cell cycle were analyzed by flow cytometry. *$P < 0.05$, $n = 3$; ***$P < 0.001$, $n = 3$. (F) Western blot analysis was used to detect the expression levels of cyclin D1 and cyclin E1 in ESCC cells treated with ivermectin (0, 5, 10, and 15 μM) for 24 h. (G) Male BALB/c nude mice were inoculated with KYSE30 cells and treated with ivermectin or vehicle. Tumor volumes were measured at the indicated time points after ivermectin treatment. *$P < 0.05$, $n = 6$; ***$P < 0.001$, $n = 6$. (H) The final tumor volumes under both control and ivermectin conditions were normalized to the initial tumor volume. *$P < 0.05$, $n = 6$. (I) Images of tumors from control or ivermectin-treated mice and tumor weights are shown when the mice were sacrificed. **$P < 0.01$, $n = 6$.

increased LC3 II conversion (Supplementary Figure S5A), indicating that the inhibition of ESCC cell growth by ivermectin is dependent on autophagy. The proportion of ivermectin-treated KYSE30 cells in the G1/G0 phase was significantly greater when they were costimulated with CQ ($P < 0.05$; Supplementary Figure S5B,D), and the percentage of apoptotic cells was significantly lower when they were costimulated with CQ ($P < 0.01$; Supplementary Figure S5C,E).

Ivermectin activates the ER stress pathway and ATF4 in ESCC cells

To investigate the molecular mechanism underlying ivermectin-mediated growth inhibition in ESCC cells, transcriptome analyses were performed via RNA-seq. The datasets generated and/or analyzed during the current study are available in the Gene Expression Omnibus (GEO, GSE201404) repository (https://www.ncbi.nlm.nih.gov/geo/query/acc.cgi?&acc=GSE201404).

Transcriptome analysis revealed 751 upregulated genes and 905 downregulated genes that occurred in both KYSE30 and KYSE70 cells after ivermectin treatment, with a one-fold expression change used as the cutoff (Supplementary Figure S6A, B). The genes in the ER stress pathway were identified as the most significantly enriched gene set or pathway through GO and KEGG analyses of the upregulated genes (Supplementary Figures S7A and S8A). The cell cycle was identified as one of the significantly enriched pathways among the downregulated genes (Supplementary Figures S7B and S8B). In addition, gene set enrichment analysis (GSEA) was performed via GSEA software (https://www.gsea-msigdb.org/gsea/index.jsp).

ATF4 was identified as a high confidence regulator in the ER stress pathway in response to ivermectin treatment (Figure 3A). The increases in the expression of ivermectin-inducible genes (*ATF4*, *CHOP*, *PERK*, *FAM129A*, *CREBRF*, *SEL1L*, *CREB3L2*, *DNAJC10*,

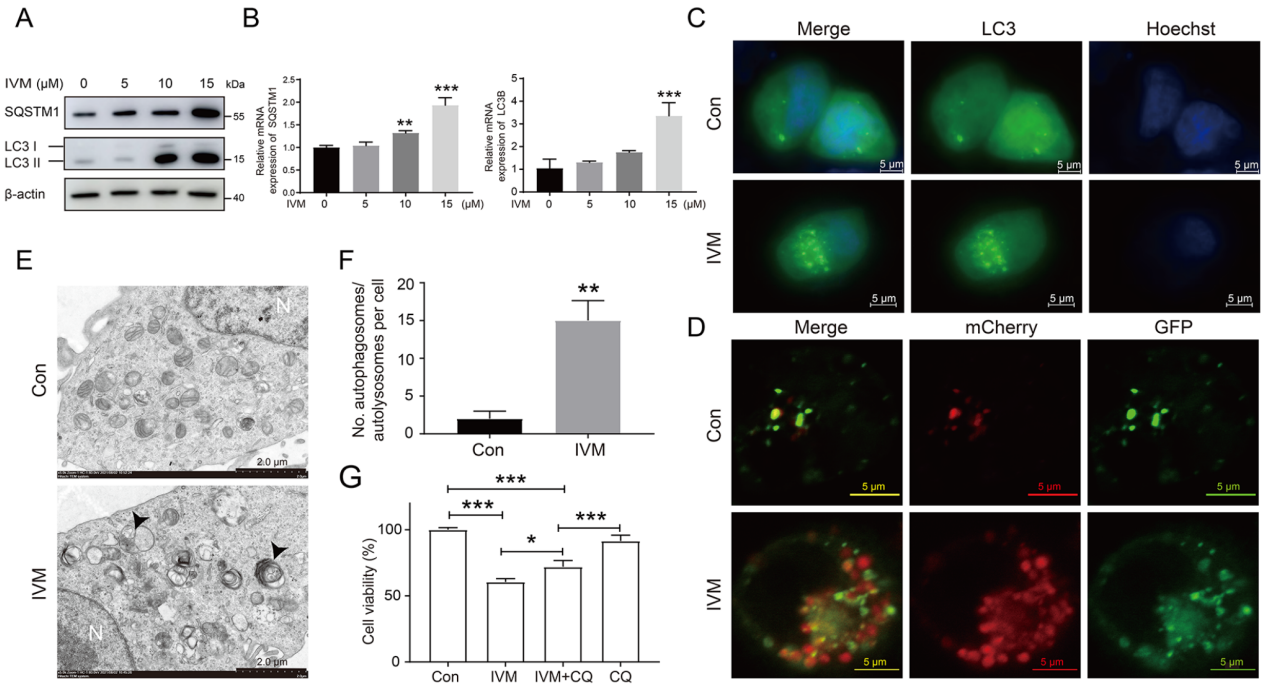

Figure 2. Ivermectin induces autophagy in ESCC cells (A) Western blot analysis was used to detect the expression levels of LC3 and p62/SQSTM1 in cells treated with the indicated concentrations of ivermectin. (B) qRT-PCR was used to analyze the expressions of *LC3B* and *p62/SQSTM1* in KYSE30 cells after ivermectin treatment. $^{**}P < 0.01$, $n = 3$; $^{***}P < 0.001$, $n = 3$. (C) Immunofluorescence staining of endogenous LC3 puncta in cells treated with 10 μM ivermectin. Scale bar: 5 μm. (D) Cells were transiently transfected with an mCherry-GFP-LC3 expression vector and treated with 10 μM ivermectin. Scale bar: 5 μm. (E) Autophagic vesicles detected by TEM in cells treated with or without ivermectin. (N, nucleus; arrows denote autophagosomes/autolysosomes). (F) The total number of autophagic vesicles was detected via TEM. $^{**}P < 0.01$, $n = 3$, scale bar: 2 μm. (G) The viability of cells treated with 10 μM ivermectin alone or in combination with 10 μM chloroquine (CQ) was detected via MTT assay. $^{*}P < 0.05$, $n = 3$; $^{***}P < 0.001$, $n = 3$.

CREB3, *WFS1*, and *OS9*) were further analyzed by qRT-PCR (Figure 3B and Supplementary Figure S9). Consistent with the notion that PERK-mediated eIF2α phosphorylation increased after ER stress, PERK phosphorylation and eIF2α phosphorylation increased after ivermectin treatment (Figure 3C and Supplementary Figure S10). Furthermore, the increase in the protein levels of PERK, CHOP, and ATF4 suggested that ER stress was induced. Moreover, western blot and qRT-PCR analyses revealed that ivermectin activated the ER stress pathway in KYSE70 cells (Figure 3D,E and Supplementary Figure S11). Consistently, the expressions of ATF4, CHOP and LC3B in ivermectin-treated xenograft tissues tended to be similar (Supplementary Figure S3D). Taken together, our results revealed that ivermectin induced ER stress and activated the PERK-ATF4-DDIT3 signaling pathway. To further investigate the relationship between ivermectin-induced ER stress and autophagy, ATF4 was overexpressed or downregulated in KYSE30 cells. Cell growth was assessed by EdU labeling and MTT assays (Figure 4). ATF4 overexpression further reduced the growth of ivermectin-treated cells (Figure 4C). The overexpression and knockout of the *ATF4* gene in KYSE30 cells were validated by western blot analysis and Sanger sequencing (Supplementary Figures S12–14).

Ivermectin induces ATF4 and autophagy through ROS generation

To further understand the cellular effects of ivermectin on ESCC cells, we evaluated the cellular ROS and calcium levels via flow cytometry. The levels of ROS in ivermectin-treated cells increased significantly (Figure 5A,B). In addition, the intracellular calcium concentration was significantly increased in KYSE30 cells after ivermectin treatment (Figure 5C,D). Moreover, the ROS scavenger tocopherol (TOC) significantly decreased the levels of ROS as well as the calcium concentration in ivermectin-treated cells (Figure 5A–D). Compared with that in the ivermectin treatment group, cell viability in the TOC and ivermectin treatment groups was significantly greater (Figure 5E). Compared with those in the ivermectin treatment group, the expressions of ATF4 and LC3 in the ivermectin and TOC treatment groups were significantly lower, as shown by both qPCR and western blot analysis (Figure 5F,G and Supplementary Figure S15). These results suggested that ivermectin affects cellular signaling pathways, including ROS and calcium levels, to elicit its biological effects on ER stress and cell death.

Discussion

Safe and effective chemotherapeutic drugs are still highly needed for current cancer treatments. One way to solve this problem is drug repurposing. Ivermectin is a promising antitumor drug repurposed from its original use [24]. During early drug development, preclinical toxicity studies of ivermectin were performed in neonatal rats and mice. The LD_{50} of ivermectin is approximately 42.8–52.8 mg/kg and 28–30 mg/kg in rats and mice, respectively [25,26]. A previous study revealed that ivermectin doses up to 2 mg/kg would be tolerable in healthy volunteers [27]. Ivermectin is administered intraperitoneally in mice at 10 mg/kg (human equivalent dose of 0.81 mg/kg, lower than 2 mg/kg) without side effects

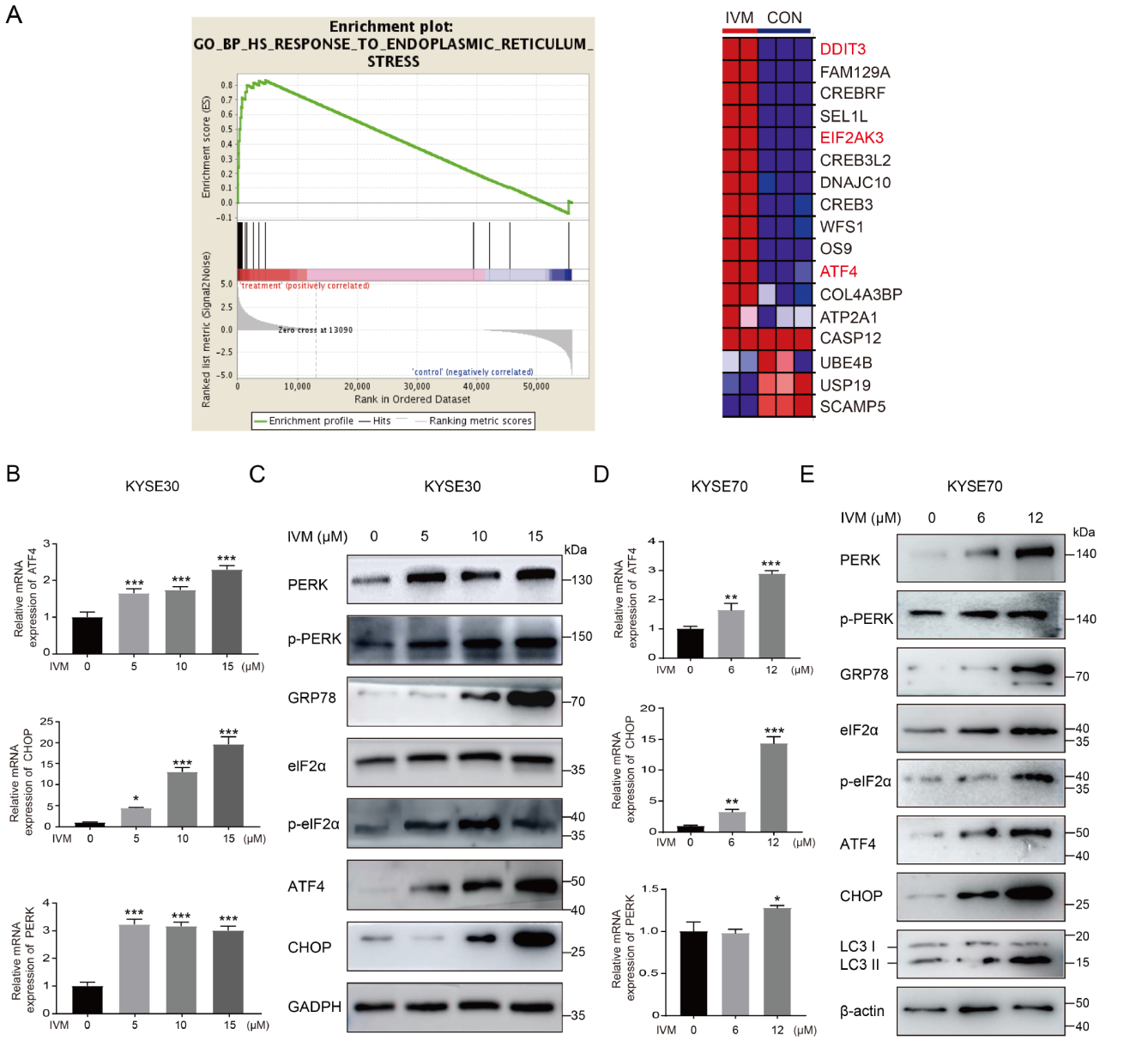

Figure 3. Ivermectin activates the ER stress pathway and induces autophagy in ESCC cells (A) GSEA of gene sets involved in ER stress, which was affected after ivermectin treatment. The normalized enrichment score (ES) is shown. The color index represents gene expression changes, and the leading edge genes are red. (B) The mRNA expression levels of *ATF4*, *DDIT3*, and *PERK* were analyzed after ivermectin treatment in KYSE30 cells. $^{*}P < 0.05$, $n = 3$; $^{***}P < 0.001$, $n = 3$. (C) Western blot analysis was used to determine the expression levels of PERK, p-PERK (Thr980), GRP78, p-eIF2α (Ser51), eIF2α, ATF4, and CHOP in KYSE30 cells treated with the indicated concentrations of ivermectin for 24 h. (D) The mRNA expression levels of *ATF4*, *DDIT3*, and *PERK* were analyzed after ivermectin treatment in KYSE70 cells. $^{*}P < 0.05$, $n = 3$; $^{**}P < 0.01$, $n = 3$; $^{***}P < 0.001$, $n = 3$. (E) Western blot analysis was used to measure the expressions of PERK, p-PERK (Thr980), GRP78, eIF2α, p-eIF2α (Ser51), ATF4, CHOP, and LC3 in KYSE70 cells treated with the indicated concentrations of ivermectin for 24 h.

and has a strong antitumor effect [28,29]. Ivermectin has been used in millions of parasite-infected patients and is well tolerated; therefore, it has been proven to be safe at its antiparasitic dosage [6]. Ivermectin was used for the treatment of *S. stercoralis* hyperinfection in a chronic lymphocytic leukemia patient [30] and for the treatment of Demodex infestation in a six-year-old child with acute lymphoblastic leukemia [31], indicating that ivermectin is a safe treatment option in cancer patients.

Unfortunately, no clinical trials of ivermectin have been reported in cancer clinical trials. Interestingly, 91 clinical trials using ivermectin for SARS-CoV-2 infection were recorded at registration sites until February 2021 [32], including a trial titled "Early treatment with ivermectin and LosarTAN for Cancer Patients With COVID-19 Infection (TITAN) (https://ClinicalTrials.gov/show/NCT04447235") [33]. The COVID-19 patients also experienced cancer in this trial, which provided accompanying clinical data concerning the anticancer effects of ivermectin.

Ivermectin can inhibit the growth of more than 50 human cancer cell lines [34]. In addition, as an anticancer drug, ivermectin does not damage normal cells and has few side effects at appropriate

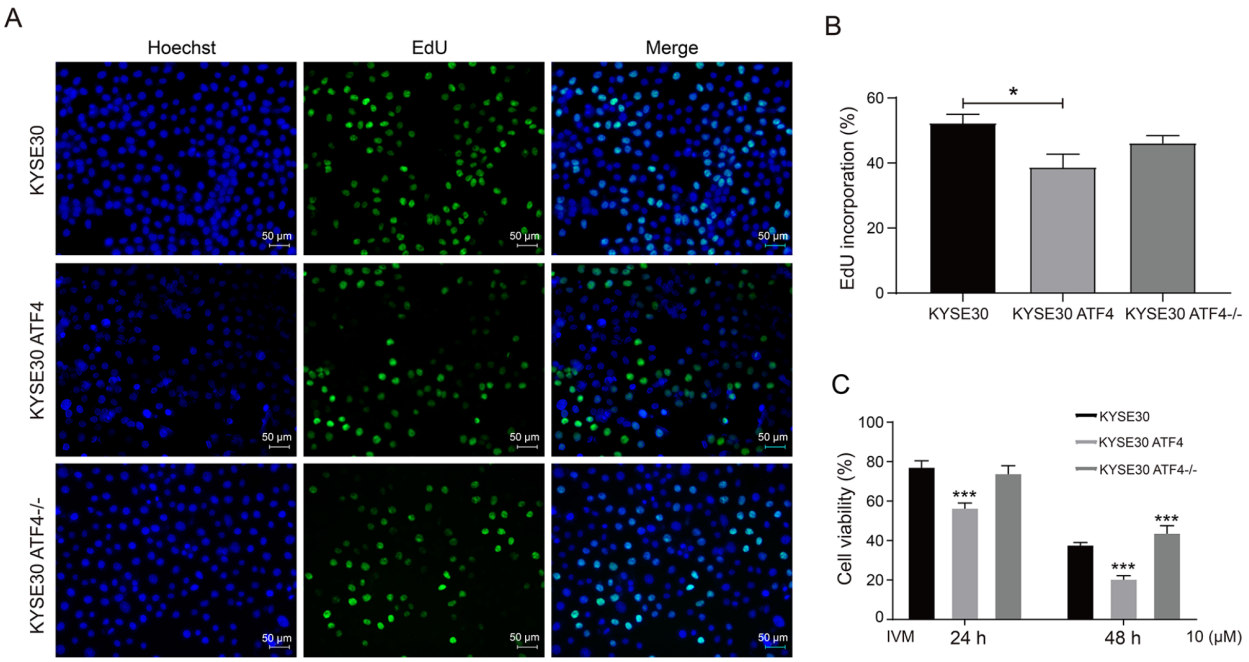

Figure 4. Ivermectin affects cell growth through ATF4 (A,B) The proliferation of KYSE30 ATF4 (ATF4-overexpressing cells), KYSE30 ATF4$^{-/-}$ (ATF4-knockout cells), and KYSE30 cells was measured via EdU labeling. *$P < 0.05$, $n = 3$. (C) The viabilities of KYSE30 ATF4 (ATF4-overexpressing cells), KYSE30 ATF4$^{-/-}$ (ATF4-knockout cells), and KYSE30 cells treated with ivermectin were detected via MTT assay. ***$P < 0.001$, $n = 3$.

doses [35]. However, the mechanisms underlying the growth inhibitory effects of ivermectin are elusive. Our study revealed that ivermectin activates ER stress by promoting ATF4 and autophagy, leading to the inhibition of tumor growth in ESCC cells.

The homeostasis of autophagy plays an important role in cancer cells. A growth-suppressive role of autophagy was observed in cancer cells treated with certain drugs [36,37]. Our study revealed that the autophagy induced by ivermectin inhibited the proliferation of ESCC cells, with no significant increase in apoptosis observed at 24 h after drug treatment. In contrast, significant apoptosis was observed at 48 h after drug treatment. Our results suggest that the autophagy induced by ivermectin may inhibit cell proliferation at early time points after ivermectin treatment and before apoptosis is induced at later time points. Previous studies have shown that ivermectin induces cytostatic autophagy in breast cancer cells [38]. Our data also revealed that ivermectin treatment for 24 h arrested cells in the G1 phase of the cell cycle rather than inducing cell death via apoptosis in ESCC cells. The mode of the cellular response to ivermectin, either cell cycle arrest, autophagy, or cell death, depends on the ivermectin concentration and duration of treatment. Thus, the antitumor role of ivermectin has not been summarized as precise and describable as its antiparasitic and antiviral effects. Ivermectin appears to effectively eliminate tumors *in vivo* at much lower doses that are non-toxic to cancer cells *in vitro* [39,40]. Consequently, whether the *in vivo* activity of ivermectin with respect to cancer is informative remains to be tested. In addition, Singh *et al.* [41] reported that ivermectin inhibits Plasmodium falciparum erythrocyte stages *in vitro*, with an IC_{50} near 0.5 μM, whereas an improved novel ivermectin analog (analog-19) had a better IC_{50} of 0.05 mM. This novel ivermectin analog with increased efficacy may improve the antitumor effect.

Our data indicated that ivermectin markedly increased the expression of ATF4 and activated the ER stress signaling pathway. Previous reports have shown that increased LC3B expression is regulated by PERK-dependent activation of ATF4 [42]. ATF4 expression and autophagy were induced by ivermectin, and the effects of ivermectin on cell viability were observed. However, the mechanism involved needs further study. Previous studies have shown that ivermectin can induce autophagy, but the detailed mechanism underlying ivermectin-mediated regulation of ATF4 has not been reported. Studies on cancer treatment have revealed that ER stress is activated by chemotherapeutic drugs. ER stress is caused by disturbances in the structure and function of the ER after hypoxia, nutrient deprivation, Ca^{2+} imbalance, protein glycosylation perturbation and ROS elevation [43–45]. We demonstrated here that ivermectin activated ER stress and increased ROS and Ca^{2+} levels in ESCC cells. Pretreatment with TOC decreased the calcium concentration in KYSE30 cells treated with ivermectin, which indicated that ROS affected calcium homeostasis. The expressions of ATF4 and LC3 were reduced, and cell viability was increased by TOC, suggesting that ROS are upstream of ER-stress and the induction of cell death. The inhibition of autophagy by CQ blocked the cell death induced by ivermectin, suggesting that autophagy promoted ivermectin-mediated cell death. Moreover, apoptosis analysis confirmed the ability of the autophagy inhibitor CQ to rescue the growth suppression induced by ivermectin. CQ enhanced G1 phase arrest in ivermectin-treated KYSE30 cells; however, the effects of ivermectin on autophagy and the cell cycle warrant further investigation. The ER is the primary cellular organelle that contains a high concentration of Ca^{2+}; therefore, the ER plays an essential role in maintaining intracellular Ca^{2+} homeostasis. Under normal conditions, the cellular calcium level ranges between 0.1 and 0.8 mM in the ER, is close to 0.1 μM in the cytosol, and is approximately 1–2 mM in the extracellular space [46]. The increase in cytosolic Ca^{2+} under ER stress conditions is involved in the initiation of the autophagy process, including vesicular induction,

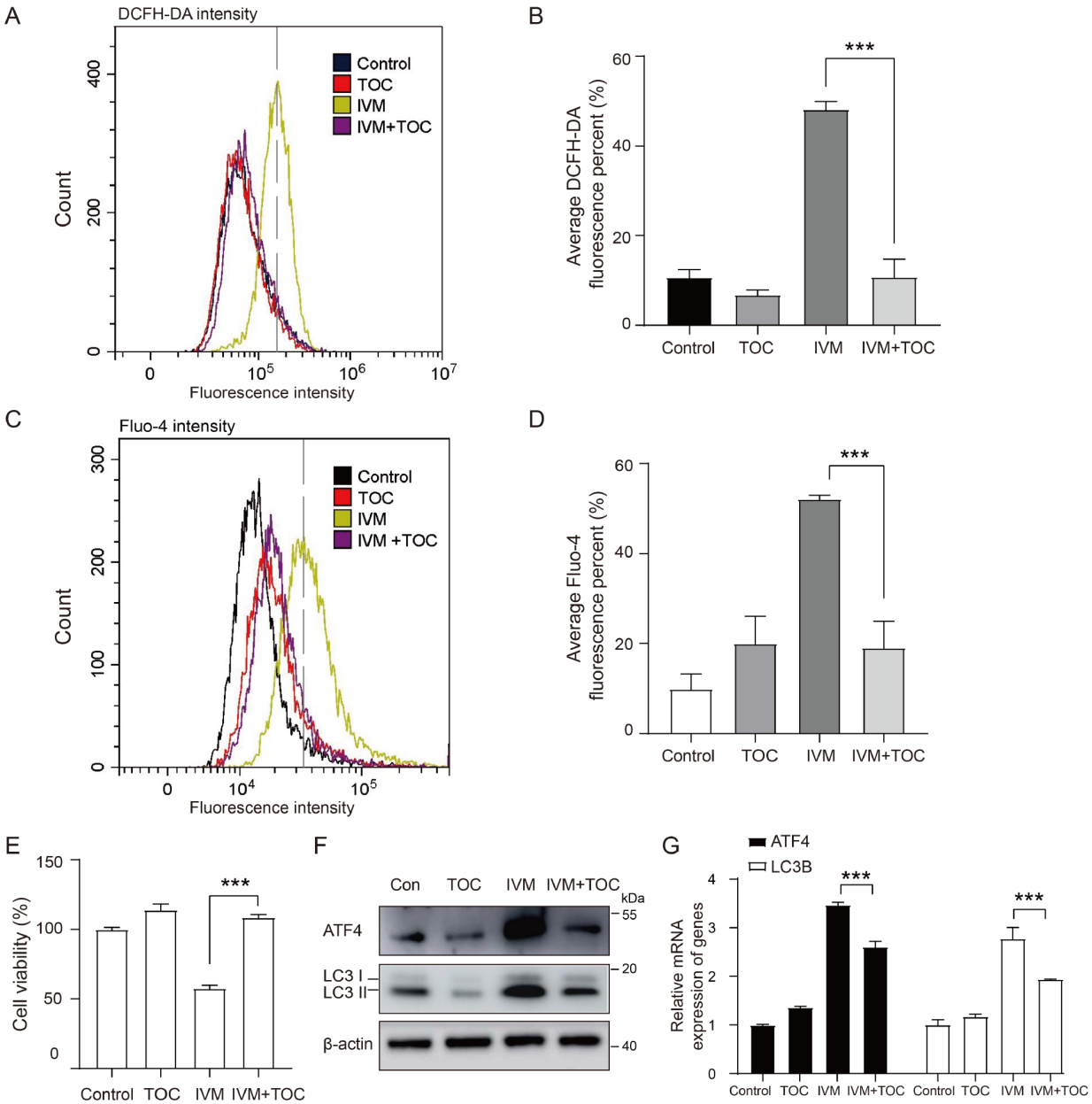

Figure 5. ROS induction and calcium concentrations in KYSE30 cells after ivermectin treatment (A,B) Cells were treated with ivermectin (10 μM) and TOC (5 mM) for 6 h and further incubated with DCFH-DA to detect intracellular ROS levels via flow cytometry. ***$P < 0.001$, $n = 3$. (C,D) Cells were treated with ivermectin (10 μM) and TOC (5 mM) for 24 h and further incubated with Fluo-4 to detect calcium concentrations via flow cytometry. ***$P < 0.001$, $n = 3$. (E) Cell viability was measured by the MTT assay in KYSE30 cells treated with ivermectin (10 μM) and TOC (5 mM). ***$P < 0.001$, $n = 3$. (F) Western blot analysis was used to measure the expressions of ATF4 and LC3 in KYSE30 cells treated with ivermectin (10 μM) or TOC (5 mM) for 24 h. (G) The mRNA expression levels of *ATF4* and *LC3B* were analyzed after ivermectin and TOC treatment in KYSE30 cells. ***$P < 0.001$, $n = 3$.

nucleation, and elongation [47]. As described in a previous work, thapsigargin induced ER stress, as well as Ca^{2+}-dependent autophagy, as analyzed by LC3 translocation and electron microscopy [14]. Ivermectin may play a similar role as thapsigargin in our work. Future studies are needed to investigate the crosstalk between ROS, Ca^{2+} signaling, ER stress, and autophagy in cells after ivermectin treatment.

In summary, our study revealed that ivermectin inhibits ESCC tumor growth by activating ATF4-dependent ER stress-autophagy. These findings provide insights into the anticancer efficacy of ivermectin, which offers preclinical evidence to support the clinical evaluation of ivermectin for the treatment of ESCC. In our future work, we will combine ivermectin with standard chemotherapeutic reagents to determine whether synergy exists.

Supplementary Data

Supplementary data is available at *Acta Biochimica et Biophysica Sinica* online.

Acknowledgements

We thank Dr Shuangyi Yin (Huaihe Hospital of Henan University) and the bioinformatics team (biotrainee) of Dr Jianming Zeng (University of Macau) for generously sharing their experience and codes.

Funding

This work was supported by the grants from the Natural Science Foundation of Henan Province of China (No. 222300420117), the Henan Provincial Science and Technology R&D Joint Fund (Industrial Category) key project (No. 235101610003), the Henan Postdoctoral Science Foundation to Mengmeng Lu, the National Natural Science Foundation of China (No. 82273173), and the Startup Funds of Henan University to Yanming Wang.

Conflict of Interest

The authors declare that they have no conflict of interest.

References

1. Sung H, Ferlay J, Siegel RL, Laversanne M, Soerjomataram I, Jemal A, Bray F. Global cancer statistics 2020: GLOBOCAN estimates of incidence and mortality worldwide for 36 cancers in 185 countries. *CA Cancer J Clin* 2021, 71: 209–249
2. Liu R, Hong R, Wang Y, Gong Y, Yeerken D, Yang D, Li J, *et al.* Defect of SLC38A3 promotes epithelial mesenchymal transition and predicts poor prognosis in esophageal squamous cell carcinoma. *Chin J Cancer Res* 2020, 32: 547–563
3. Chen W, Zheng R, Zhang S, Zeng H, Xia C, Zuo T, *et al.* Cancer incidence and mortality in China, 2013. *Cancer Lett* 2017, 401: 63–71
4. Li L, Liu M, Lin JB, Hong XB, Chen WX, Guo H, Xu LY, *et al.* Diagnostic value of autoantibodies against ezrin in esophageal squamous cell carcinoma. *Dis Markers* 2017, 2017: 1–6
5. Martin RJ, Robertson AP, Choudhary S. Ivermectin: an anthelmintic, an insecticide, and much more. *Trends Parasitology* 2021, 37: 48–64
6. Jittamala P, Monteiro W, Smit MR, Pedrique B, Specht S, Chaccour CJ, *et al.* A systematic review and an individual patient data meta-analysis of ivermectin use in children weighing less than fifteen kilograms: is it time to reconsider the current contraindication? *PLoS Negl Trop Dis* 2021, 15: e0009144
7. Crump A. Ivermectin: enigmatic multifaceted 'wonder' drug continues to surprise and exceed expectations. *J Antibiot* 2017, 70: 495–505
8. Formiga FR, Leblanc R, de Souza Rebouças J, Farias LP, de Oliveira RN, Pena L. Ivermectin: an award-winning drug with expected antiviral activity against COVID-19. *J Control Release* 2021, 329: 758–761
9. Wagstaff KM, Sivakumaran H, Heaton SM, Harrich D, Jans DA. Ivermectin is a specific inhibitor of importin α/β-mediated nuclear import able to inhibit replication of HIV-1 and dengue virus. *Biochem J* 2012, 443: 851–856
10. Juarez M, Schcolnik-Cabrera A, Dueñas-Gonzalez A. The multitargeted drug ivermectin: from an antiparasitic agent to a repositioned cancer drug. *Am J Cancer Res* 2018, 8: 317–331
11. Lv S, Wu Z, Luo M, Zhang Y, Zhang J, Pascal LE, Wang Z, *et al.* Integrated analysis reveals FOXA1 and Ku70/Ku80 as targets of ivermectin in prostate cancer. *Cell Death Dis* 2022, 13: 754
12. Mizushima N, Yoshimori T, Levine B. Methods in mammalian autophagy research. *Cell* 2010, 140: 313–326
13. Johansson I, Monsen VT, Pettersen K, Mildenberger J, Misund K, Kaarniranta K, Schønberg S, *et al.* The marine n-3 PUFA DHA evokes cytoprotection against oxidative stress and protein misfolding by inducing autophagy and NFE2L2 in human retinal pigment epithelial cells. *Autophagy* 2015, 11: 1636–1651
14. Høyer-Hansen M, Jäättelä M. Connecting endoplasmic reticulum stress to autophagy by unfolded protein response and calcium. *Cell Death Differ* 2007, 14: 1576–1582
15. Salimi L, Akbari A, Jabbari N, Mojarad B, Vahhabi A, Szafert S, Kalashani SA, *et al.* Synergies in exosomes and autophagy pathways for cellular homeostasis and metastasis of tumor cells. *Cell Biosci* 2020, 10: 64
16. Ji G, Yu N, Xue X, Li Z. PERK-mediated autophagy in osteosarcoma cells resists ER stress-induced cell apoptosis. *Int J Biol Sci* 2015, 11: 803–812
17. Lim B, Greer Y, Lipkowitz S, Takebe N. Novel apoptosis-inducing agents for the treatment of cancer, a new arsenal in the toolbox. *Cancers* 2019, 11: 1087
18. Zhao Y, Yu Y, Li H, Zhang Z, Guo S, Zhu S, Guo Q, *et al.* FAM175B promotes apoptosis by inhibiting ATF4 ubiquitination in esophageal squamous cell carcinoma. *Mol Oncol* 2019, 13: 1150–1165
19. Wang S, Chen XA, Hu J, Jiang J, Li Y, Chan-Salis KY, Gu Y, *et al.* ATF4 gene network mediates cellular response to the anticancer PAD inhibitor YW3-56 in triple-negative breast cancer cells. *Mol Cancer Ther* 2015, 14: 877–888
20. Kasai S, Yamazaki H, Tanji K, Engler MJ, Matsumiya T, Itoh K. Role of the ISR-ATF4 pathway and its cross talk with Nrf2 in mitochondrial quality control. *J Clin Biochem Nutr* 2019, 64: 1–12
21. Sarcinelli C, Dragic H, Piecyk M, Barbet V, Duret C, Barthelaix A, Ferraro-Peyret C, *et al.* ATF4-dependent NRF2 transcriptional regulation promotes antioxidant protection during endoplasmic reticulum stress. *Cancers* 2020, 12: 569
22. Luhr M, Torgersen ML, Szalai P, Hashim A, Brech A, Staerk J, Engedal N. The kinase PERK and the transcription factor ATF4 play distinct and essential roles in autophagy resulting from tunicamycin-induced ER stress. *J Biol Chem* 2019, 294: 8197–8217
23. Lu M, Xiong D, Sun W, Yu T, Hu Z, Ding J, Cai Y, *et al.* Sustained release ivermectin-loaded solid lipid dispersion for subcutaneous delivery: *in vitro* and *in vivo* evaluation. *Drug Deliver* 2017, 24: 622–631
24. Tang M, Hu X, Wang Y, Yao X, Zhang W, Yu C, Cheng F, *et al.* Ivermectin, a potential anticancer drug derived from an antiparasitic drug. *Pharmacol Res* 2021, 163: 105207
25. Crump A, Omura S. Ivermectin, 'Wonder drug' from Japan: the human use perspective. *Proc Jpn Acad Ser B* 2011, 87: 13–28
26. Sharmeen S, Skrtic M, Sukhai MA, Hurren R, Gronda M, Wang X, Fonseca SB, *et al.* The antiparasitic agent ivermectin induces chloride-dependent membrane hyperpolarization and cell death in leukemia cells. *Blood* 2010, 116: 3593–3603
27. Guzzo CA, Furtek CI, Porras AG, Chen C, Tipping R, Clineschmidt CM, Sciberras DG, *et al.* Safety, tolerability, and pharmacokinetics of escalating high doses of ivermectin in healthy adult subjects. *J Clin Pharma* 2002, 42: 1122–1133
28. Reagan-shaw S, Nihal M, Ahmad N. Dose translation from animal to human studies revisited. *FASEB J* 2008, 22: 659–661
29. Melotti A, Mas C, Kuciak M, Lorente-Trigos A, Borges I, Ruiz i Altaba A. The river blindness drugI vermectin and related macrocyclic lactones inhibit WNT-TCF pathway responses in human cancer. *EMBO Mol Med* 2014, 6: 1263–1278
30. Wilkin A, Palavecino E, Guerrero-Wooley R, Aranda-Aguirre E, Li W. Case report: strongyloides stercoralis hyperinfection in a patient with chronic lymphocytic leukemia. *Am J Tropical Med Hyg* 2017, 97: 1629
31. Damian D, Rogers M. *Demodex* infestation in a child with leukaemia: treatment with ivermectin and permethrin. *Int J Dermatol* 2003, 42: 724–726

32. Yagisawa M, Hanaki H. Global trends in clinical studies of ivermectin in COVID-19. *The Japanese Journal of Antibiotics* 2021, 74: 44–95
33. Jans DA, Wagstaff KM. Ivermectin as a broad-spectrum host-directed antiviral: the real deal? *Cells* 2020, 9: 2100
34. Juarez M, Schcolnik-Cabrera A, Dominguez-Gomez G, Chavez-Blanco A, Diaz-Chavez J, Duenas-Gonzalez A. Antitumor effects of ivermectin at clinically feasible concentrations support its clinical development as a repositioned cancer drug. *Cancer Chemother Pharmacol* 2020, 85: 1153–1163
35. Zhu M, Li Y, Zhou Z. Antibiotic ivermectin preferentially targets renal cancer through inducing mitochondrial dysfunction and oxidative damage. *Biochem Biophys Res Commun* 2017, 492: 373–378
36. Liu R, Li J, Zhang T, Zou L, Chen Y, Wang K, Lei Y, ***et al.*** Itraconazole suppresses the growth of glioblastoma through induction of autophagy. *Autophagy* 2014, 10: 1241–1255
37. Liu Y, Levine B. Autosis and autophagic cell death: the dark side of autophagy. *Cell Death Differ* 2015, 22: 367–376
38. Dou Q, Chen HN, Wang K, Yuan K, Lei Y, Li K, Lan J, ***et al.*** Ivermectin induces cytostatic autophagy by blocking the PAK1/Akt axis in breast cancer. *Cancer Res* 2016, 76: 4457–4469
39. Draganov D, Han Z, Rana A, Bennett N, Irvine DJ, Lee PP. Ivermectin converts cold tumors hot and synergizes with immune checkpoint blockade for treatment of breast cancer. *npj Breast Cancer* 2021, 7: 22
40. Draganov D, Gopalakrishna-Pillai S, Chen YR, Zuckerman N, Moeller S, Wang C, Ann D, ***et al.*** Modulation of P2X4/P2X7/Pannexin-1 sensitivity to extracellular ATP via Ivermectin induces a non-apoptotic and inflammatory form of cancer cell death. *Sci Rep* 2015, 5: 16222
41. Singh L, Fontinha D, Francisco D, Mendes AM, Prudêncio M, Singh K. Molecular design and synthesis of ivermectin hybrids targeting hepatic and erythrocytic stages of *plasmodium* parasites. *J Med Chem* 2020, 63: 1750–1762
42. Rzymski T, Milani M, Pike L, Buffa F, Mellor HR, Winchester L, Pires I, ***et al.*** Regulation of autophagy by ATF4 in response to severe hypoxia. *Oncogene* 2010, 29: 4424–4435
43. Feng Y, Yang Y, Fan C, Di S, Hu W, Jiang S, Li T, ***et al.*** Pterostilbene inhibits the growth of human esophageal cancer cells by regulating endoplasmic reticulum stress. *Cell Physiol Biochem* 2016, 38: 1226–1244
44. Park H, Song G, Lim W. Ivermectin-induced programmed cell death and disruption of mitochondrial membrane potential in bovine mammary gland epithelial cells. *Pesticide Biochem Physiol* 2020, 163: 84–93
45. Beck D, Niessner H, Smalley KSM, Flaherty K, Paraiso KHT, Busch C, Sinnberg T, ***et al.*** Vemurafenib potently induces endoplasmic reticulum stress–mediated apoptosis in BRAFV600E melanoma cells. *Sci Signal* 2013, 6: ra7
46. Samtleben S, Jaepel J, Fecher C, Andreska T, Rehberg M, Blum R. Direct imaging of ER calcium with targeted-esterase induced dye loading (TED). *J Vis Exp* 2013
47. Song S, Tan J, Miao Y, Zhang Q. Crosstalk of ER stress-mediated autophagy and ER-phagy: involvement of UPR and the core autophagy machinery. *J Cell Physiol* 2018, 233: 3867–3874